Constrained-MMSE Combining for Spatial Domain Self-Interference Cancellation in Full-Duplex Massive MIMO Systems

XUAN CHEN [1,2,3], VINCENT SAVAUX [1] (Senior Member, IEEE),
MATTHIEU CRUSSIÈRE [1,2] (Member, IEEE), PATRICK SAVELLI [1],
AND KOFFI-CLÉMENT YAO [4] (Member, IEEE)

[1]Advanced Connectivity Lab, Institute of Research and Technology b<>com, 35510 Rennes, France
[2]IETR, INSA Rennes, 35700 Rennes, France
[3]BU TowerCo, TDF, 75015 Paris, France
[4]Lab-STICC CNRS UMR 6285, 29238 Brest, France

CORRESPONDING AUTHOR: X. CHEN (e-mail: xuan.chen@b-com.com)

ABSTRACT This paper introduces a novel spatial domain-based self-interference cancellation (SIC) method named constrained minimum mean square error (C-MMSE) for massive multiple-input multiple-output (mMIMO) full-duplex (FD) communication systems. The main idea involves treating the self-interference (SI) signal emitted from an FD node as a distinct spatial stream arriving at the receiver part of that same FD node. This SI signal needs to be spatially postcoded alongside other relevant signals coming from different transmitters, ensuring it falls into the null space of the MIMO channel, which includes the FD node transmitter part as an input. To establish this approach, we first adapt the expressions of spatial combiners for conventional zero forcing (ZF) and minimum mean square error combining (MMSE) criteria. We demonstrate that MMSE alone is insufficient for efficient SI signal cancellation unless an additional constraint is added to enable proper SIC. Consequently, we design the innovative C-MMSE combiner and derive its expression. In addition to our proposal, the originality of our work stems from employing a spherical wave model (SWM) to model the SI channel. The choice is justified by the proximity of the transmit and receive antenna panels in the FD node. We examine and compare the SIC performance of the modified ZF combiner, the modified MMSE combiner, and the newly introduced C-MMSE combiner by evaluating the spectral efficiency (SE). Additionally, we highlight the robustness of the SWM-based SI channel modeling in comparison to conventional planar wave modeling (PWM), emphasizing the relevance of its usage.

INDEX TERMS Full-duplex, hybrid beamforming, MIMO, MMSE postcoding, self-interference cancellation, spherical wave channel model, ZF postcoding.

I. INTRODUCTION

FULL duplex (FD) is one of the most promising techniques to meet the ever-growing need for data rate in future wireless communications, applications, and services [1]. FD is theoretically able to double the overall capacity of radio links between transceivers compared to usual half-duplex (HD) communications, either in frequency or time. To this end, transceivers must have the capability to transmit and receive signals at the same time and in the same frequency band [1], [2], [3], [4], [5], which is still a pending technical challenge for practical implementations. However, in the last decade, FD has gained interest in various applications and technologies, such as wireless fidelity (WiFi) [6] or relaying [7], [8], [9]. In fifth-generation (5G) networks, FD has been suggested as a solution for integrated access & backhaul (IAB) systems [10], [11] to cope with the densification of the networks. Additionally, non-overlapping sub-band FD (SBFD) is proposed to improve uplink (UL) throughput performance [12]. More recently, the authors of [13] mentioned the use case of integrated sensing

and communications (ISAC) in the context of 6G, which inherently requires an FD transceiver to receive the sounding signals while transmitting data to other devices.

Although FD opens new perspectives in wireless communications, it suffers from self-interference (SI) that inevitably occurs since the transmitter is prone to radiate in the direction of the co-localized receivers. In some conditions of high path loss attenuation, typically observed in mmWave communications, the signal of interest (SOI) may be concealed in the SI and cannot be properly decoded. This makes the FD technique unsuitable for reliable communications. As a consequence, numerous self-interference cancellation (SIC) techniques have been developed to overcome this downside. According to [1], [14], [15], the SIC techniques can be classified into three categories depending on the physical domain where SIC is applied: the propagation, the analog, and the digital domains. The propagation domain includes all SIC methods based on the properties of electromagnetic wave propagation and antenna isolation [16], [17], [18], [19]. SIC in analog and digital domains is based on signal processing, where the interfering signal is estimated and then subtracted from the received signal [20], [21], [22]. The residual SI is then digitally mitigated through iterative processes, for instance [23], [24], [25]. It is worth emphasizing that the SIC techniques in the three domains are independent and can be applied to complement each other.

In recent years, a new spatial SIC domain has emerged with the development of (massive) multi-input multi-output ((m)MIMO) systems [7], [8], [26], [27]. In fact, the use of multiple antennas allows for the formation of signal beams employing analog, digital, or hybrid (both analog and digital) precoding (resp. combiner or postcoding) at the transmitter side (resp. receiver). Such beamforming is a promising solution for SIC in MIMO systems and can also be combined with the aforementioned techniques.

While a majority of existing works considered the use of beamforming techniques offered by MIMO to enhance the performance of FD systems [9], [11], [27], [28], [29], [30], the core of those SIC methods still resumes in the conventional digital domain suppression method, where a replica of the SI signal is created and subtracted from the actual received signal. One main drawback of this approach is the requirement of a strict time domain synchronization between the replica and the actual received signal. Any minor mismatches between these two signals may result in a degradation of the overall performance of the system. The authors in [8] suggested a block diagonalization approach to perform spatial domain SIC using a digital beamforming scheme. Such a method is, however, only applicable in FD relay scenarios where the relay node, operating in FD, receives a signal from another node and simultaneously transmits a signal to another. In this paper, we consider a more generic FD system in which the node, operating in FD, not only transmits a signal to another node but also simultaneously receives signals from both a third node and nearby user equipments (UEs). Due to the more general system model we consider in our study, those methods used in FD relay scenarios [5], [23], [26], [27], [29] can not be applied in our case.

In this paper, we propose an entirely spatial domain-based SIC method relying on a hybrid beamforming MIMO architecture to deal with the UEs UL case of our generic FD system model. Without loss of generality, we assume a multi-carrier signal as the baseline waveform. Spatial SIC is then performed in the spatial domain using digital beamforming for each subcarrier. Additionally, analog beamforming is applied in the time domain at the radio front-end. With such SIC architecture, no SI signal subtraction is applied to the received signal. Instead, a postcoding operation is employed, thus avoiding the synchronization issues associated with conventional time domain SIC methods. Furthermore, unlike conventional beamforming-based SIC algorithms as those considered in FD relay literature [7], [8], [9], our approach relies on integrating the SI signal as one particular spatial stream between the T_x and R_x of the FD node. This allows the digital spatial combiner to properly perform SIC. Another originality of our work is the use of the spherical wave model (SWM) to characterize the SI channel, in contrast to the approach taken in most other works [9], [10], [11], [29]. Since the FD node uses two closely placed antenna arrays for transmission and reception, the spherical wave model (SWM) proves to be more appropriate than the conventional planar wave model (PWM) for MIMO systems. This choice is supported by empirical measurements [31] and theoretical findings [32].

Based on our generic system model, we initiate our study by adapting the expressions for the well-known zero-forcing (ZF) and minimum mean square error (MMSE) combiners. In particular, we theoretically demonstrate that the naively modified MMSE combiner is not capable of handling the SI, and additional constraints need to be considered to enable the MMSE combiner to perform SIC properly. After deriving the theoretical expression of this new constrained MMSE (C-MMSE) combiner, we evaluate the performance of the modified ZF and C-MMSE approaches via simulation to show the relevance of our proposal and the efficiency of the proposed FD system architecture. Since the use of network-controlled repeaters (NRC) by IAB may be one of the possible use cases of our considered model, we use the same formalism as those used in IAB systems. Thus, the links between the nodes are called backhaul (BH) links, and the links between the node and UEs are called access links. Note that in the current version of Rel-18 of 3GPP, only single-hop NRC is studied [33]. However, our considered model may serve as a potential solution for multiple-hop NRC in a later release.

Eventually, the main contributions of this paper can be summarized as:

- We propose a spatial domain-based SIC strategy for UL FD systems, relying on a hybrid beamforming

MIMO architecture and multi-carrier waveform. In this approach, digital combiners can be employed to treat the SI signals, thereby avoiding the time domain synchronization issue.

- We adapt the conventional ZF and MMSE beamforming schemes to our considered system model, referred to as modified ZF and modified MMSE in the sequel. Additionally, we propose and derive the expression of a new combiner, called C-MMSE, designed to perfectly cancel the SI. The latter is shown to outperform the two former methods, both theoretically and through simulations.

- We compare the SI channel modeling based on the SWM with the channel modeling based on the PWM and demonstrate the robustness and accuracy of the former through simulations.

The rest of the paper is organized as follows: Section II presents the different channel models considered in our system. Section III provides a preliminary study of the system model, followed by Section IV, which discusses the modified system model and introduces our spatial SIC combiner. Section V presents the simulation parameters and results, and Section VI concludes our work, providing insights for future works.

Notations: Boldface letters a and normal font letters a represent vectors and scalars, respectively. Capital boldface letters A represents matrices. A^T, A^H, and $tr(A)$ represents the transpose operation of matrix A, the conjugate transpose operation of matrix A, and the trace of matrix A, respectively. $\|.\|_2$ and $\|.\|_F$ denote the L2-norm and the Frobenius norm, respectively. $\mathbb{E}[.]$ denotes the mathematical expectation function.

II. CHANNEL MODEL FOR UPLINK FD SCENARIO

We consider in this paper the uplink (UL) case for UEs, where the node of interest (indexed with 1) is receiving signals from another node (indexed with 0) and UEs located in the cell. In addition, node 1 simultaneously transmits a signal to a third node (indexed with 2). Without loss of generality, we assume that all the nodes employ uniform planar arrays (UPA) with a $\frac{\lambda}{2}$ spacing for both reception and transmission. The next sections describe the different channel models we use in our work. Fig. 1 provides a global view of all the different channels involved in our model. In Fig. 1, the solid arrows represent the line of sight (LOS) component of a signal, while the dashed arrows represent the non-line of sight (NLOS) component of a signal due to the presence of the scatterers. Note that in Fig. 1, we consider two separated antenna arrays for transmission and reception at node 1 to keep the model as general as possible, but it is also possible to consider a shared antenna array for both T_x and R_x. Furthermore, in our considered UL communication scenario, the R_x (resp. T_x) of node 0 (resp. node 2) do not interact with node 1. Therefore, we choose not to present them in Fig. 1.
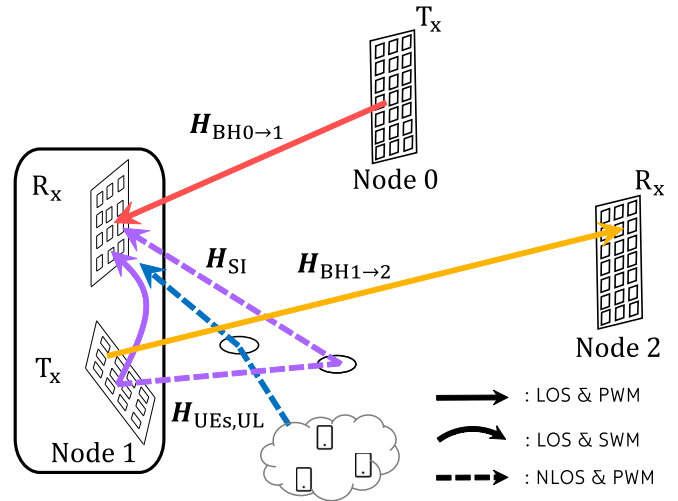

FIGURE 1. Overview of all the considered channels related to node 1.

A. SELF-INTERFERENCE CHANNEL

As mentioned in the introduction, the main issue of an FD system is the presence of SI. The SI signal results from the transmission of the signal dedicated to node 2 by node 1, but it is also received by the very same node 1. This occurs through a particular SI channel corresponding to the propagation environment between the T_x and R_x antennas of the node. Thus, proper modeling of the SI channel is crucial for SIC. In literature, many authors consider this channel as a multipath NLOS channel with a high Ricean K-factor [10], [11], [34]. The latter consideration is reasonable since, in FD systems, the distance between the T_x and the R_x parts is very small. Consequently, the power of the LOS path (represented by the solid purple arrow in Fig. 1) directly emitted from the T_x is very strong compared to the other NLOS paths (represented by the dashed purple arrow in Fig. 1). However, in most existing works, many authors only assume the channel model as a PWM, which is not rigorously exact, considering the close proximity of the transmitter and the receiver. In fact, as shown in [32], the SI channel model would be more accurately represented if the SWM is considered. Very few works, such as [30], consider the channel model as a SWM due to the modeling difficulty. In our work, we adopt the assumption that the channel consists only of a LOS contribution, and the NLOS contribution due to nearby scatterers is negligible. Furthermore, inspired by the work of [35], we adopt the following SWM of the SI channel $H_{\mathrm{SI},m,n}$ between the mth R_x antenna and the nth T_x antenna:

$$H_{\mathrm{SI},m,n} = \rho e^{j\phi} \frac{D}{D_{m,n}} e^{-j\frac{2\pi}{\lambda}\Delta_{\mathrm{SWM},m,n}}, \qquad (1)$$

with $\rho e^{j\phi}$ the complex gain expressing the channel between the center O_{T_x} of the T_x antenna array and the center O_{R_x} of the R_x antenna array. $\frac{D}{D_{m,n}}$ represents an amplitude fluctuation term due to the small distance between the T_x and R_x antennas, where D is the distance between O_{T_x}
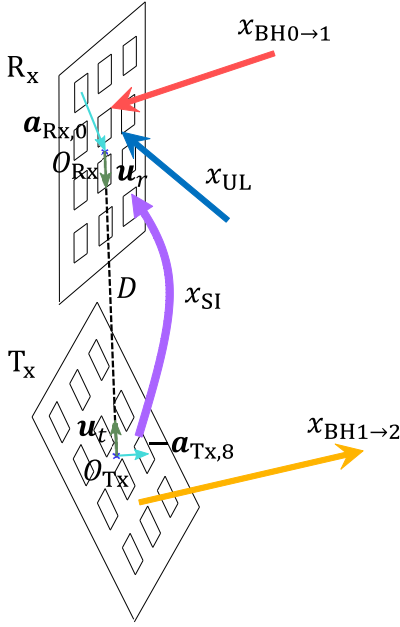
FIGURE 2. 3D view of the geometry between the T_x and R_x of node 1.

and O_{R_x}, and $D_{m,n}$ is the distance between the center of the mth antenna of the R_x antenna array and the center of the nth antenna of the T_x antenna array. λ corresponds to the wavelength, and $\Delta_{SWM} \triangleq D_{m,n} - D$ represents the phase shift with respect to the reference points located at O_{T_x} and O_{R_x} defined as:

$$\Delta_{SWM,m,n} = \| -a_{T_x,n} + Du_t + Ra_{R_x,m} \|_2 - D, \quad (2)$$

with $-a_{T_x,n}$ the vector from the nth antenna of the T_x array to the center O_{T_x}, Du_t the vector from O_{T_x} to O_{R_x}, R the rotation matrix mapping the vectors of the R_x coordinate into the T_x coordinate: $Ru_r = u_t$, and $a_{R_x,m}$ the vector from the center O_{R_x} to the mth antenna of the R_x array. Fig. 2 provides a detailed 3D view of the previously described geometry for the transceiver of node 1. In Fig. 2, an example of two 3×4 UPA structures is considered for the transceiver of node 1. In particular, we provide an example of the vectors $a_{T_x,n}$ (resp. $a_{R_x,m}$) in the case where $n = 8$ (resp. $m = 0$).

B. BACKHAUL CHANNEL

The second type of channel we have to consider is the BH channel. In the considered architecture, there are two BH channels related to node 1. First, let us define channel $H_{BH0\rightarrow1}$ as the BH channel between node 0 and node 1 to receive the BH signal from the node 0 (see Fig. 1). Note that the indices of nodes 0 and 2 are arbitrary since they are interchangeable. Then, let us denote $H_{BH1\rightarrow2}$ the BH channel between the node 1 and the node 2. In practice, the antenna arrays are installed almost on top of the base station (BS), thus, very few obstacles would be present at that altitude. Hence, we adopt a pure LOS planar wave channel model for both BH channels $H_{BH0\rightarrow1}$ and $H_{BH1\rightarrow2}$, even though it

could be generalized to NLOS channels as well. The channel construction is done through a ray-based model, as in [36], which only requires the steering vector of the T_x part and the R_x part. The channel matrices of the BH links are thus given by:

$$H_{BH0\rightarrow1} = \beta_{0\rightarrow1} e_{R_x}^{(1)}\left(\phi_{BH}^{(0)}, \theta_{BH}^{(0)}\right) e_{T_x}^{(0)}\left(\phi_{BH}^{(0)}, \theta_{BH}^{(0)}\right)^H, \quad (3)$$

$$H_{BH1\rightarrow2} = \beta_{1\rightarrow2} e_{R_x}^{(2)}\left(\phi_{BH}^{(1)}, \theta_{BH}^{(1)}\right) e_{T_x}^{(1)}\left(\phi_{BH}^{(1)}, \theta_{BH}^{(1)}\right)^H, \quad (4)$$

$$\beta_{0\rightarrow1} = \sqrt{M_{T_x,BH}^{(0)} M_{R_x,BH}^{(1)}}\left(\frac{\lambda}{4d_{0\rightarrow1}}\right), \quad (5)$$

$$\beta_{1\rightarrow2} = \sqrt{M_{T_x,BH}^{(1)} M_{R_x,BH}^{(2)}}\left(\frac{\lambda}{4d_{1\rightarrow2}}\right), \quad (6)$$

with $\beta_{0\rightarrow1}$ (resp. $\beta_{1\rightarrow2}$) the free space path loss factor for channel $H_{BH0\rightarrow1}$ (resp. $H_{BH1\rightarrow2}$), $d_{0\rightarrow1}$ (resp. $d_{1\rightarrow2}$) the distance between node 0 and 1 (resp. 1 and 2). $e_{T_x}^{(0)}$ of dimension $M_{T_x,BH}^{(0)} \times 1$ represents the steering vector of the T_x of node 0, where $M_{T_x,BH}^{(0)}$ is the number of antennas of the T_x array of node 0 dedicated to sending the BH signal to node 1. Similarly, $e_{R_x}^{(1)}$ and $e_{T_x}^{(1)}$, both of dimensions $M_{R_x,BH}^{(1)} \times 1$ and $M_{T_x,BH}^{(1)} \times 1$, respectively, represent the steering vector of the R_x and T_x of node 1. Here, $M_{R_x,BH}^{(1)}$ and $M_{T_x,BH}^{(1)}$ correspond to the numbers of antennas in the R_x and T_x arrays of node 1 dedicated to receiving the BH signal from node 0 and sending the BH signal to node 2. $e_{R_x}^{(2)}$, with dimension $M_{R_x,BH}^{(2)} \times 1$, represents the steering vector of the R_x of node 2, where $M_{R_x,BH}^{(2)}$ is the number of antennas in the R_x array of node 2 dedicated to receiving the BH signal from node 1. Additionally, $\theta_{BH}^{(0)}$ (resp. $\phi_{BH}^{(0)}$) represents the azimuth (resp. elevation) angle of the direction of departure (DoD) of the antennas in the T_x array of node 0, while $\theta_{BH}^{(1)}$ (resp. $\phi_{BH}^{(1)}$) is the azimuth (resp. elevation) angle of the DoD of the antennas in the T_x array of node 1. Note that, since we consider our antenna arrays to be UPAs with $\frac{\lambda}{2}$ spacing, the expression of (5) and (6) are simplified. It is also worth noticing that, since we consider a pure LOS path between the different nodes, the angles of the DoD of the T_x of node 0 (respectively 1) are the same as the angles of the direction of arrival (DoA) of the R_x of node 1 (respectively 2). From this construction, the dimension of the channel matrix $H_{BH0\rightarrow1}$ is $M_{R_x,BH}^{(1)} \times M_{T_x,BH}^{(0)}$, and the dimension of the channel matrix $H_{BH1\rightarrow2}$ is $M_{R_x,BH}^{(2)} \times M_{T_x,BH}^{(1)}$. Note that the expression of the components of the steering vectors is detailed later in the section regarding the design of analog precoder/combiner in Section III.

C. ACCESS LINK CHANNEL

The last type of channel in our system model is the channel between node 1 and the K_1 UEs around the node. In practice, the UEs are randomly located around the node, and due to the environment, a certain number of scatterers would be unavoidable in the design of this channel. In this case, We adopt a NLOS PWM for the modeling (represented by
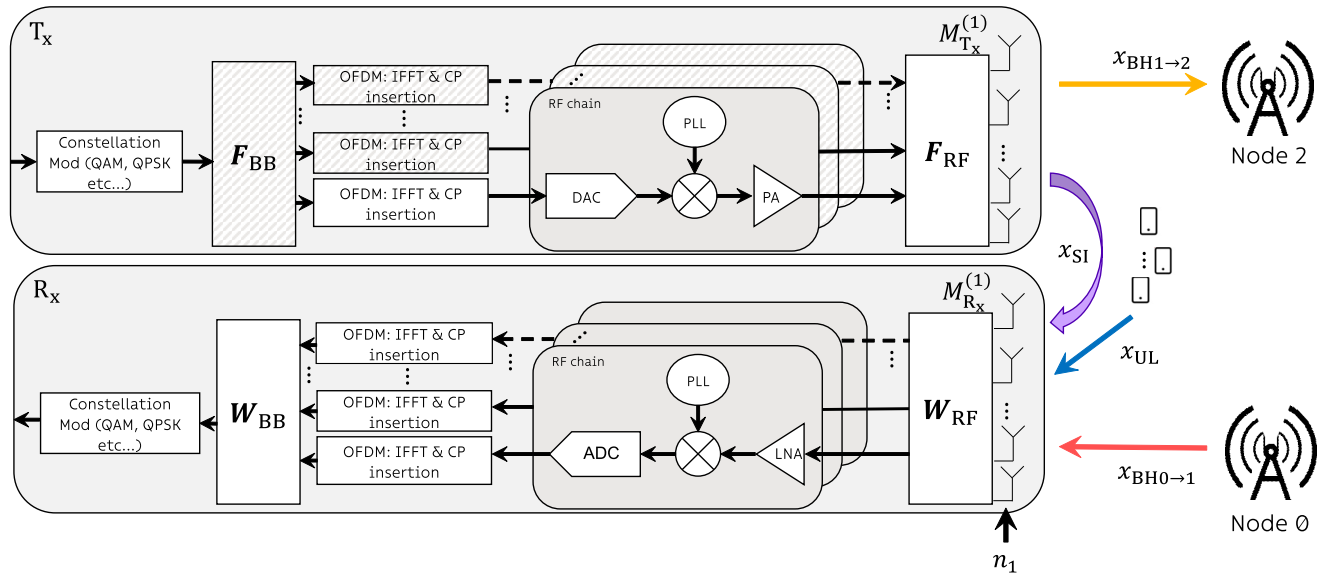
FIGURE 3. Hybrid beamfomring architecture of the UL scenario.

the dashed blue arrow in Fig. 1). The construction of the channel is done through the L-ray-based model, as described in [36]. In this model, we consider there is one direct ray from the kth UE toward the R_x of node 1. Subsequently, we construct $L-1$ other rays with a DoD separated by an angle of $\frac{\Delta\theta}{L}$ and $-\frac{\Delta\theta}{L}$ for both elevation and azimuth compared to the main ray. This way, there are L angles of departure from each UE, and the angle of arrival at the antennas of the R_x of node 1 is randomly taken from $[-\pi; \pi]$ for elevation and $[-\frac{\pi}{2}; \frac{\pi}{2}]$ for azimuth to simulate the scattering environment. Note that, for simplification, we consider all the UEs to only have one single isotropic antenna, meaning that UEs do not have the possibility to perform any analog or digital beamforming. This assumption could be straightforwardly generalized to multiple antennas UEs. Thus, the number of antennas around node 1, denoted as K_1, corresponds to the number of UEs around node 1, and the channel matrix can be constructed column by column, where each column represents the transmission of one UE. The uth column of the channel matrix for the UEs UL situation is then given by the following equation:

$$\boldsymbol{H}_{\text{UEs,UL},u} = \sum_{l=0}^{L-1} \alpha_l e^{-j2\pi f \tau_l} \boldsymbol{e}_{R_x,u}(\phi_u, \theta_u), \qquad (7)$$

with L being the number of paths induced by the presence of scatterers, α_l the complex attenuation coefficient for the lth path, τ_l the delay associated with the lth path, $\boldsymbol{e}_{R_x,u}$ the steering vector of R_x of node 1 with dimension $M_{R_x,\text{UE},u} \times 1$ associated with the uth UE, θ_u and ϕ_u being the angle of azimuth and elevation, respectively, representing the position of the uth UE as seen from the node side. From this construction, the dimension of the channel matrix $\boldsymbol{H}_{\text{UEs,UL}}$ is $M_{R_x,\text{UE}}^{(1)} \times K_1$.

III. SYSTEM MODEL: PRELIMINARY STUDY WITHOUT SIC

In this section, we introduce our generic hybrid beamforming FD system model, emphasizing the SI component that requires attention. As a preliminary study, however, this SI component is treated as an external interference term. Consequently, the baseband (BB) combiner is designed to accommodate the received SI term but its primary purpose is not to strictly perform SIC.

A. HYBRID BEAMFORMING FD SYSTEM MODEL FOR UL SCENARIO

Fig. 3 depicts the FD hybrid beamforming transceiver for node 1. Both T_x and R_x share typical blocks found in FD transceivers, including modulation constellation, orthogonal frequency-division multiplexing (OFDM) modulation, and radio-frequency (RF) chain, as outlined in the work of [37]. In addition to these components, hybrid beamforming is employed, meaning that both BB treatment and RF treatment are jointly used to form beams. However, in the UL scenario, where only a BH signal is sent to node 2 by the T_x part of node 1, only one RF chain is activated. Consequently, the digital precoder $\boldsymbol{F}_{BB}$ is also disabled. In a more generic scenario, where node 0 sends multiple BH signals to various nodes, the digital precoder $\boldsymbol{F}_{BB}$ would be activated, along with different RF chains at the T_x side. For the sake of clarity and simplicity, we limit our analysis to the single BH signal case in the following sections. The receive signal model is thus given by:

$$\begin{aligned} \boldsymbol{y} &= \boldsymbol{W}_{BB}^H \boldsymbol{W}_{RF}^H \hat{\boldsymbol{H}} \hat{\boldsymbol{F}}_{RF,\text{eq}} \hat{\boldsymbol{P}} \hat{\boldsymbol{x}} \\ &\quad + \boldsymbol{W}_{BB}^H \boldsymbol{W}_{RF}^H \boldsymbol{H}_{SI} \boldsymbol{e}_{BH1\rightarrow 2}^{(1)} \sqrt{P_{SI}} x_{SI} + \boldsymbol{W}_{BB}^H \boldsymbol{W}_{RF}^H \boldsymbol{n} \\ &= \boldsymbol{W}_{BB}^H \hat{\boldsymbol{z}}. \end{aligned} \qquad (8)$$
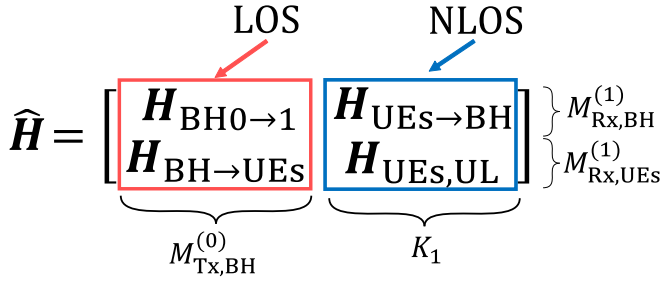
FIGURE 4. Global UL scenario channel construction (without proposed SIC solution).

in (8), where the SI signal is considered as additional noise added to the reception of the SOI, $\hat{H}$ represents the global channel matrix of dimension $(M_{\mathrm{R_x,BH}}^{(1)} + M_{\mathrm{R_x,UEs}}^{(1)}) \times (M_{\mathrm{T_x,BH}}^{(0)} + K_1)$ constructed by concatenating the previously defined channels as shown in Fig. 4. Also, $\hat{P} = \mathrm{diag}(\sqrt{P_{\mathrm{BH0}\to1}}, \sqrt{P_{\mathrm{UE0}}}, \ldots, \sqrt{P_{\mathrm{UE}K_1-1}})$ is the 4×4 diagonal power allocation matrix for all the transmitters of the scenario, except for the $\mathrm{T_x}$ of node 1. P_{SI} is the power allocated by the $\mathrm{T_x}$ of node 1 to send the BH signal x_{SI} to node 2. Hence P_{SI} represents the power of SI in this scenario. Finally, $\hat{x} = (x_{\mathrm{BH0}\to1}, x_{\mathrm{UE0}}, \ldots, x_{\mathrm{UE}K_1-1})^T$ is the $(K_1 + 1) \times 1$ vector gathering the transmitted signal from all the transmitters except the $\mathrm{T_x}$ of node 1.

As illustrated in Fig. 4, the global channel is realistically modeled by incorporating interference channels, denoted as $H_{\mathrm{BH}\to\mathrm{UEs}}$ (resp. $H_{\mathrm{UEs}\to\mathrm{BH}}$) into the matrix $\hat{H}$. These channels account for the communication between the $\mathrm{T_x}$ antennas of node 0 (resp. the antennas of UEs around node 1) that are dedicated to transmitting the BH signal to node 1 (resp. the UEs' UL signal to node 1) and the $\mathrm{R_x}$ antennas of node 1 that are dedicated to receiving the UEs' UL signal (resp. the BH signal from node 0).

B. RF PRECODER/COMBINER DESIGN
In this section, we focus on the design of the RF precoder and the equivalent RF combiner. Our design employs UPAs with a $\frac{\lambda}{2}$ spacing, and the expression for the steering vector is given by:

$$e_k = \alpha \begin{bmatrix} 1 \\ e^{-j\pi(\sin(\phi_k)+\sin(\theta_k)\cos(\phi_k))} \\ \vdots \\ e^{-j\pi\left((M_{k,V}^{(i)}-1)\sin(\phi_k)+\sin(\theta_k)\cos(\phi_k)\right)} \\ \vdots \\ e^{-j\pi\left((M_{k,V}^{(i)}-1)\sin(\phi_k)+(M_{k,H}^{(i)}-1)\sin(\theta_k)\cos(\phi_k)\right)} \end{bmatrix}, \quad (9)$$

with $\alpha = \frac{1}{\sqrt{M_{x,k}^{(i)}}}$ the normalization factor depending on the number of $\mathrm{T_x}$ or $\mathrm{R_x}$ antennas ($x \in \{\mathrm{T_x, R_x}\}$) of the ith node ($i \in \{0, 1, 2\}$). k is the direction index taking value in $\{\mathrm{BH0} \to 1, \mathrm{UE0}, \ldots, \mathrm{UE}K_1-1\}$. ϕ_k (resp. θ_k) corresponds to the elevation (resp. azimuth) angle of the direction k.

$M_{k,V}^{(i)}$ (resp. $M_{k,H}^{(i)}$) is the number of rows (resp. columns) of elementary antennas dedicated to the direction k on the $\mathrm{T_x}$ or $\mathrm{R_x}$ array of node i. For a matter of clarity, we note e_k ($k \in \{\mathrm{BH0} \to 1, \mathrm{UE0}, \ldots, \mathrm{UE}K_1-1\}$) instead of $e_k(\phi_k, \theta_k)$ for all the steering vectors. The expression of the analog combining matrix W_{RF} can then be determined as follows:

$$W_{\mathrm{RF}} = \begin{bmatrix} e_{\mathrm{BH0}\to1} & 0 & \cdots & 0 \\ 0 & e_{\mathrm{UE0}} & \cdots & \vdots \\ \vdots & \vdots & \cdots & \vdots \\ 0 & \cdots & \cdots & e_{\mathrm{UE}K_1-1} \end{bmatrix}, \quad (10)$$

with $e_{\mathrm{BH0}\to1}$ the steering vector of size $M_{\mathrm{R_x,BH}}^{(1)} \times 1$ pointing towards the direction of $\mathrm{T_x}$ of node 0, and $e_{\mathrm{UE}j}$ the steering vector of size $M_{\mathrm{R_x,UE}j}^{(1)} \times 1$ pointing towards the direction of the jth UEs ($j \in \{0, \ldots, K_1-1\}$). Since W_{RF} considers all the antennas of $\mathrm{R_x}$ of node 1, the dimension of W_{RF} is $M_{\mathrm{R_x}}^{(1)} \times (K_1+1)$. Without loss of generality, we assume that a beam steering operation was previously performed at node 1, providing the latter with perfect knowledge (or at least an excellent estimation through a beam alignment procedure) of the position of UEs and the other nodes.

After obtaining the expression for the analog combining matrix W_{RF}, the next consideration is the global transmitter in the UL scenario. In this case, we concatenate the steering vectors of all the different transmitters to form the equivalent analog precoding matrix $\hat{F}_{\mathrm{RF,eq}}$:

$$\hat{F}_{\mathrm{RF,eq}} = \begin{bmatrix} e_{\mathrm{BH0}\to1} & 0 \\ 0 & \vdots \\ \vdots & \vdots \\ 0 & I_{K_1} \end{bmatrix}. \quad (11)$$

Here, $e_{\mathrm{BH0}\to1}$ represents the steering vector of size $M_{\mathrm{T_x,BH}}^{(0)} \times 1$ pointing towards the direction of the $\mathrm{T_x}$ of node 1, and I_{K_1} denotes the $K_1 \times K_1$ identity matrix, reflecting the inability of the K_1 UEs around node 1 to perform any beamforming. It is noteworthy that the dimension of $\hat{F}_{\mathrm{RF,eq}}$ is $(M_{\mathrm{T_x,BH}}^{(0)} + K_1) \times (K_1 + 1)$.

C. BASEBAND COMBINER DESIGN
To address the BB processing W_{BB}, we first define the $(K_1 + 1) \times (K_1+1)$ equivalent channel matrix, including the effects of analog precoding and combining:

$$\hat{H}_{\mathrm{eq}} = W_{\mathrm{RF}}^H \hat{H} \hat{F}_{\mathrm{RF,eq}}. \quad (12)$$

From (8), it becomes apparent that the digital combiner W_{BB} is unable to simultaneously mitigate the effect of H_{eq} and H_{SI}. Thus, there is no need to consider the well-known ZF combiner in this case, as its effect is not comprehensive. Nevertheless, it is viable to explore an MMSE combiner, which addresses the effects of both H_{eq} and H_{SI} concurrently, as follows:

$$\arg\min_{W_{\mathrm{BB}}} \mathbb{E}\left[\|\hat{P}\hat{x} - W_{\mathrm{BB}}^H z\|_F^2\right]. \quad (13)$$

The resolution of (13) leads to:

$$W_{BB} = \left(\hat{H}_{eq}\hat{H}_{eq}^H + \sigma^2 I\right)^{-1}\left(\hat{H}_{eq} - D_{x_{SI}x_{SI}}\right), \quad (14)$$

with

$$D_{x_{SI}x_{SI}} = H_{SI,eq}H_{SI,eq}^H p_{SI}, \quad (15)$$

and

$$H_{SI,eq} = W_{RF}^H H_{SI} e_{BH1\to2}^{(1)}. \quad (16)$$

However, the so-constructed W_{BB} is not able to strictly cancel the SI, a fact that can be translated mathematically as:

$$W_{BB}^H H_{SI,eq} \neq \mathbf{0}. \quad (17)$$

The mathematical reason behind this characteristic is that, as the SI signal is considered as separate noise for the system, the equivalent SI channel $H_{SI,eq}$ has no direct connection with the equivalent channel matrix $\hat{H}_{eq}$. Consequently, in the resulting matrix $W_{BB}^H H_{SI,eq}$, the contribution of SI remains non-null. We hereby understand that to properly cancel the SI, it is necessary to consider the SI as an intrinsic part of the transmitted signal in the system model. In the next section, we propose a modified system model designed to appropriately address SIC.

IV. PROPOSED HYBRID BEAMFORMING SOLUTION WITH SIC

We now enhance the previous system model by incorporating the SI channel into the global channel matrix $\hat{H}$ and integrating the transmitted SI signal $x_{BH1\to2}$ into the vector $\hat{x}$. The underlying idea is to represent the interference component as a term embedded in the received signal, with the intention of granting the digital combiner cancellation capability.

A. MODIFIED SYSTEM MODEL

Thus, the received signal at R_x of node 1 can be rewritten in a more compact form:

$$\begin{aligned} y &= W_{BB}^H W_{RF}^H H F_{RF,eq} P x + W_{BB}^H W_{RF}^H n \\ &= W_{BB}^H z, \end{aligned} \quad (18)$$

with $x = (x_{BH1\to2}, x_{BH0\to1}, x_{UE0}, \ldots, x_{UEK_1-1})^T$ the newly constructed vector of the transmitted signal from all the T_x, including that of node 1 of the considered scenario. $P = \text{diag}(\sqrt{P_{BH1\to2}}, \sqrt{P_{BH0\to1}}, \sqrt{P_{UE0}}, \ldots, \sqrt{P_{UEK_1-1}})$ is the diagonal power allocation matrix, gathering the allocated power for all the transmitted signal at each T_x side. Note that the definition in (18) is mathematically equivalent to the definition in (8). However, (18) physically considers the SI signal as an intrinsic signal within the system model, which is not the case in (8). The global channel matrix H is shown in Fig. 5, where the additional first bloc on the left side represents the contribution of the SI channel. It is worth mentioning that, since we include the contribution of the SI signal into the other signals, the dimension of vector x is $(K_1 + 2) \times 1$ instead of $(K_1 + 1) \times 1$ for $\hat{x}$.
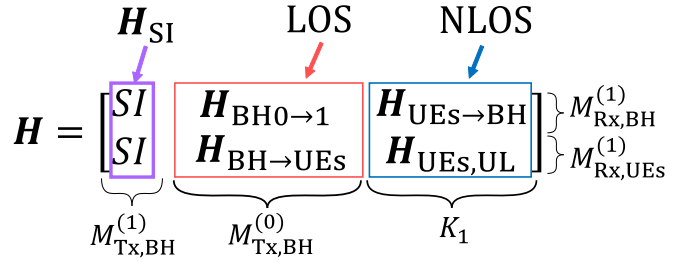

FIGURE 5. Global UL scenario channel construction (Proposed hybrid beamforming SIC solution).

B. RF PRECODER/COMBINER DESIGN

The RF combiner and equivalent precoder in our proposed solution are constructed in the same way as in the preliminary study presented in Section III. By concatenating different steering vectors by column, the expression of W_{RF} remains identical to the one presented previously. However, since we now include the SI signal in vector x, we also include the steering vector corresponding to the latter for the construction of $F_{RF,eq}$. Thus, the newly constructed $F_{RF,eq}$ can be determined as follows:

$$F_{RF,eq} = \begin{bmatrix} e_{BH0\to1} & \cdots & \mathbf{0} \\ \mathbf{0} & e_{BH1\to2} & \vdots \\ \vdots & \vdots & \vdots \\ \mathbf{0} & \cdots & I_{K_1} \end{bmatrix}, \quad (19)$$

where $e_{BH0\to1}$ is the steering vector corresponding to the BH signal sent from node 1 to 2, which also represents the SI signal for node 1. In the same manner as mentioned earlier, we form the equivalent channel matrix H_{eq} with dimension $(K_1 + 1) \times (K_1 + 2)$ thanks to the newly defined equivalent analog precoder $F_{RF,eq}$:

$$H_{eq} = W_{RF}^H H F_{RF,eq}. \quad (20)$$

C. BASEBAND COMBINER DESIGN

The next step of our design is to derive the digital combining matrix W_{BB} which effectively cancels the SI. As detailed below, three different strategies are proposed. The first two are direct adaptations of the conventional ZF and MMSE criteria, whereas the third one introduces a new MMSE approach with constraints, as outlined in this paper.

1) MODIFIED ZF COMBINER

As the SI channel H_{SI} is now integrated into the global channel matrix H in the proposed system model, it is now possible to define a modified ZF combining method to simultaneously attenuate the effect of the SI channel and the other channels of the system model. The definition of our proposed modified ZF combining matrix then yields:

$$\begin{aligned} W_{BB,ZF} &= \left(\eta A_{ZF} H_{eq}^H (H_{eq}H_{eq}^H)^{-1}\right)^H \\ &= \left(\eta A_{ZF} H_{eq}^+\right)^H, \end{aligned} \quad (21)$$

with $\eta = \frac{1}{\sqrt{\mathrm{tr}(\boldsymbol{H}_{\mathrm{eq}}^{+}\boldsymbol{H}_{\mathrm{eq}}^{+H})}}$ and $\boldsymbol{A}_{\mathrm{ZF}}$ the ZF objective matrix for SIC defined as:

$$\boldsymbol{A}_{\mathrm{ZF}} = \begin{bmatrix} 0 & 1 & 0 & \cdots & 0 \\ 0 & 0 & 1 & \cdots & 0 \\ \vdots & \vdots & \ddots & \cdots & \vdots \\ 0 & \cdots & \cdots & \cdots & 1 \end{bmatrix}. \tag{22}$$

The objective matrix $\boldsymbol{A}_{\mathrm{ZF}}$ is a vertical concatenation, consisting of a column vector of dimension $(K_1 + 1) \times 1$ composed solely of 0, followed by an identity matrix of dimension $(K_1 + 1) \times (K_1 + 1)$. The purpose of the first column of 0 in $\boldsymbol{A}_{\mathrm{ZF}}$ is to nullify the contribution of the SI signals transmitted from $\mathrm{T_x}$ of node 1 at the $\mathrm{R_x}$ side of node 1. Simultaneously, the identity matrix, adjacent to the first row of $\boldsymbol{A}_{\mathrm{ZF}}$, ensures that all other receivers in the system model only receive their desired signals without any inter-user interference.

The effect of the proposed modified ZF combining can be written in its matrix form as in (23), as shown at the bottom of the page. From (23), the proposed ZF hybrid beamforming scheme effectively cancels the SI arising from the transmitted signal from node 1. Consequently, the $\mathrm{R_x}$ of node 1 only receives the BH signal from node 0 alone with noise. Note that unlike most digital SIC methods that require perfect synchronization through subtraction between the received signal and its digital replica, our method mathematically accomplishes SIC with the aid of the first column of 0 in the first matrix on the right-hand side of (23). Physically, this eliminates the need for synchronization as Tx and Rx are collocated. Additionally, the proposed ZF combiner also guarantees that the $\mathrm{R_x}$ of node 2 and the K_1 UEs only receive their SOI without any inter-user interference. However, as is common with strict interference cancellation criterion, the useful power may decrease, as indicated by a potentially weak term η.

2) MODIFIED MMSE COMBINER

Let us now consider the case of the MMSE criterion to form a combiner that aims to strike a balance between achieving perfect SIC and minimizing the degradation of useful power. Traditionally, this method gives rise to a weighting term in the combiner expression, which depends on the signal-to-noise ratio (SNR). However, in our case, considering the specificity of our system model, the MMSE precoder can not be straightforwardly obtained from the generic MMSE expression. Instead, it needs to be formally derived as explained hereafter.

By applying the MMSE criterion the following optimization problem can be formulated as:

$$\boldsymbol{W}_{\mathrm{BB,MMSE}} = \underset{\boldsymbol{W}_{\mathrm{BB}}}{\arg\min}\ \mathbb{E}\left[\|\hat{\boldsymbol{P}}\hat{\boldsymbol{x}} - \boldsymbol{W}_{\mathrm{BB}}^{H}\boldsymbol{z}\|_F^2 \right]. \tag{24}$$

By examining the derivative with respect to $\boldsymbol{W}_{\mathrm{BB}}$ in (24) and carrying out some straightforward developments, we can derive the expression for the modified MMSE:

$$\boldsymbol{W}_{\mathrm{BB,MMSE}} = \left(\boldsymbol{H}_{\mathrm{eq}}\boldsymbol{H}_{\mathrm{eq}}^{H} + \sigma^2\boldsymbol{I} \right)^{-1}\boldsymbol{H}_{\mathrm{eq}}\boldsymbol{A}_{\mathrm{ZF}}^{T}. \tag{25}$$

We remark that, despite the difference in the system model compared to the existing works, the distinction between the modified MMSE combiner and the classic one only lies in the objective matrix $\boldsymbol{A}_{\mathrm{ZF}}$. In the Appendix, we show that the MMSE combiner constructed as in (25) is cannot perform SIC like the ZF combiner. This outcome is expected, as in the definition of MMSE, such as in (24), $\boldsymbol{W}_{\mathrm{BB,MMSE}}$ will only mitigate the effect of the received noise at $\mathrm{R_x}$ of node 1 but it does not explicitly express the need to cancel the SI. Therefore, a certain amount of constraints could be added to (24) to force the MMSE combiner to mitigate both the effects of noise and SI simultaneously. Consequently, we introduce a new method called C-MMSE in the following.

3) CONSTRAINED MMSE COMBINER

We now consider the same objective function as the MMSE criterion in (24). However, this time, we explicitly express the need for SIC through different constraints. We adopt the same idea as in the definition of (22), where the strict cancellation of the effect of the SI signal at each RF chain of node 1 is achieved thanks to the first column of 0 in the resulting matrix $\boldsymbol{W}_{\mathrm{BB,ZF}}^{H}\boldsymbol{H}_{\mathrm{eq}}$ of (23). The constraints can then be mathematically translated to ensure that each coefficient of the first column of the resulting matrix $\boldsymbol{W}_{\mathrm{BB}}^{H}\boldsymbol{H}_{\mathrm{eq}}$ is equal to 0. We hence refer to the so-formed MMSE combiner as the C-MMSE, highlighting the addition of explicit SIC constraints within the conventional MMSE problem formulation. With this in mind, we propose the following optimization problem with constraints O_1 for the C-MMSE combiner:

$$O_1: \begin{cases} \underset{\boldsymbol{W}_{\mathrm{BB}}}{\arg\min} & \mathbb{E}[\|\hat{\boldsymbol{P}}\hat{\boldsymbol{x}} - \boldsymbol{W}_{\mathrm{BB}}^{H}\boldsymbol{z}\|_F^2] \\ s.t. & \boldsymbol{j}_k^T\boldsymbol{W}_{\mathrm{BB}}^{H}\boldsymbol{H}_{\mathrm{eq}}\boldsymbol{c}_0 = 0\ (c_k) \\ & \forall k \in \{0, \ldots, K_1\} \end{cases}, \tag{26}$$

with $\boldsymbol{j}_k = (0, \ldots, 1, \ldots, 0)^T$ the $(K_1 + 1) \times 1$ vector with only a 1 at the kth position, and $\boldsymbol{c}_0 = (1, 0, \ldots, 0)^T$ the

$$\begin{bmatrix} y_{\mathrm{BH0 \to 1}} \\ y_{\mathrm{UE0}} \\ \vdots \\ y_{\mathrm{UE}K_1-1} \end{bmatrix} = \underbrace{\begin{bmatrix} 0 & \eta & 0 & \cdots & 0 \\ 0 & 0 & \eta & \cdots & 0 \\ \vdots & \vdots & \vdots & \ddots & \vdots \\ 0 & \cdots & \cdots & \cdots & \eta \end{bmatrix}}_{\boldsymbol{W}_{\mathrm{BB,ZF}}^{H}\boldsymbol{H}_{\mathrm{eq}}} \begin{bmatrix} \sqrt{P_{\mathrm{BH1 \to 2}}}x_{\mathrm{BH1 \to 2}} \\ \sqrt{P_{\mathrm{BH0 \to 1}}}x_{\mathrm{BH0 \to 1}} \\ \sqrt{P_{\mathrm{UE0}}}x_{\mathrm{UE0}} \\ \vdots \\ \sqrt{P_{\mathrm{UE}K_1-1}}x_{\mathrm{UE}K_1-1} \end{bmatrix} + \boldsymbol{W}_{\mathrm{BB}}^{H}\boldsymbol{W}_{\mathrm{RF}}^{H} \begin{bmatrix} n_{\mathrm{BH0 \to 1}} \\ n_{\mathrm{UE0}} \\ \vdots \\ n_{\mathrm{UE}K_1-1} \end{bmatrix} \tag{23}$$

$(K_1 + 2) \times 1$ vector with only a 1 at its first position. The role of vector c_0 is to extract the first column of $W_{BB}^H H_{eq}$, while the role of j_k is to extract the kth ($\forall k \in \{0, \dots, K_1\}$) row of the latter. The constraints defined in this manner will force each coefficient of the first column of the resulting matrix to be null. In this sense, the so-formed W_{BB} is not only able to mitigate the effect of noise but also to completely eliminate the SI.

Proposition 1: For the equality constrained optimization problem O_1, the local optimal solution is expressed as

$$W_{BB,C-MMSE} = \left(H_{eq} H_{eq}^H + \sigma^2 I \right)^{-1} H_{eq} A_{C-MMSE}^T, \quad (27)$$

with A_{C-MMSE} defined as:

$$A_{C-MMSE} = \begin{bmatrix} -\frac{\alpha_0}{\Gamma} & 1 & 0 & \cdots & 0 \\ -\frac{\alpha_1}{\Gamma} & 0 & 1 & \cdots & 0 \\ \vdots & \vdots & \vdots & \ddots & \vdots \\ -\frac{\alpha_{K_1}}{\Gamma} & 0 & \cdots & \cdots & 1 \end{bmatrix}, \quad (28)$$

α_i ($\forall i \in \{0, \dots, K_1\}$) defined as:

$$\alpha_i = j_i^T A_{ZF} H_{eq}^H \left(H_{eq} H_{eq}^H + \sigma^2 I \right)^{-1} H_{eq} c_0, \quad (29)$$

and Γ defined as:

$$\Gamma = c_0^T H_{eq}^H \left(H_{eq} H_{eq}^H + \sigma^2 I \right)^{-1} H_{eq} c_0. \quad (30)$$

Proof: Given that both the objective function and the constraints in the optimization problem O_1 are convex, we employ the classical Lagrangian multiplier method to solve this problem. Let μ_k be the Lagrangian multiplier for the kth constraint ($k \in \{0, \dots, K_1\}$), the Lagrangian function $\mathcal{L}$ can be defined as follows:

$$\mathcal{L}\left(W_{BB}, \mu_0, \dots, \mu_{K_1} \right) = \mathbb{E}\left[\| \hat{P}\hat{x} - W_{BB}^H z \|_F^2 \right]$$
$$+ \sum_{k=0}^{K_1} \mu_k j_k^T W_{BB}^H H_{eq} c_0. \quad (31)$$

Thanks to the complex matrix derivation formulas in [38] and [39], we can derive the following expression for W_{BB}:

$$\frac{\partial \mathcal{L}}{\partial W_{BB}^*} = 0$$
$$\Leftrightarrow W_{BB} = \left(H_{eq} H_{eq}^H + \sigma^2 I \right)^{-1}$$
$$\cdot \left(H_{eq} A_{ZF}^T - \sum_{k=0}^{K_1} \mu_k H_{eq} c_0 j_k^T \right). \quad (32)$$

We can substitute W_{BB} into the ith ($\forall i \in \{0, \dots, K_1\}$) constraint of (26) using (32) to determine the value of the ith Lagrangian multiplier μ_i, by solving:

$$j_i^T \left(A_{ZF} H_{eq}^H - \sum_{k=0}^{K_1} \mu_k j_k c_0^T H_{eq}^H \right)$$
$$\cdot \left(H_{eq} H_{eq}^H + \sigma^2 I \right)^{-1} H_{eq} c_0 = 0(c_i). \quad (33)$$

Noticing that the expression in (33) involves the difference between two scalars, (33) can also be written as:

$$\alpha_i - \left(\sum_{k=0}^{K_1} \mu_k j_i^T j_k c_0^T H_{eq}^H \right) \left(H_{eq} H_{eq}^H + \sigma^2 I \right)^{-1} H_{eq} c_0 = 0, \quad (34)$$

where α_i is defined in (29). It is also worth noticing that $j_i^T j_k = \delta_{ik}$, with δ_{ik} being the Kronecker delta function (which equals to 1 only for $i = k$ and 0 when $i \neq k$). Keeping that in mind, (34) can be further simplified as:

$$\alpha_i - \mu_i c_0^T H_{eq}^H \left(H_{eq} H_{eq}^H + \sigma^2 I \right)^{-1} H_{eq} c_0 = 0, \quad (35)$$

which leads to:

$$\mu_i = \frac{\alpha_i}{c_0^T H_{eq}^H \left(H_{eq} H_{eq}^H + \sigma^2 I \right)^{-1} H_{eq} c_0} = \frac{\alpha_i}{\Gamma}, \quad (36)$$

where Γ is a scalar defined in (30). The final expression of the C-MMSE combiner is then given as follows:

$$W_{BB,C-MMSE} = \left(H_{eq} H_{eq}^H + \sigma^2 I \right)^{-1}$$
$$\left(H_{eq} A_{ZF}^T - \sum_{k=0}^{K_1} \frac{\alpha_k}{\Gamma} H_{eq} c_0 j_k^T \right)$$
$$= \left(H_{eq} H_{eq}^H + \sigma^2 I \right)^{-1} H_{eq} A_{C-MMSE}^T, \quad (37)$$

$\blacksquare$

The proposed C-MMSE combiner is very similar to the modified MMSE combiner previously found in (25), with the main difference lying in the objective function. In the objective matrix A_{C-MMSE}, the contribution of the $K_1 + 1$ constraints is present in the first column to explicitly cancel the effect of the SI signal. In contrast, in (25), there is only a first column of 0. The effect of the proposed C-MMSE combiner can be expressed as follows:

$$W_{BB,C-MMSE}^H H_{eq} c_0 = \mathbf{0}, \quad (38)$$

which means that our proposed C-MMSE combiner is capable of completely canceling the effect of the SI signal at R_x of node 1. The proof of (38) is provided in the Appendix. The next section provides simulation results to justify all the theoretical analyses we have conducted.

V. SIMULATIONS AND DISCUSSIONS
A. SIMULATION PARAMETERS
In this section, simulation results are obtained through numerical computations to evaluate the relevance of our proposed hybrid beamforming method.

Table 1 presents all the used simulation parameters. We consider a UL scenario with 3 UEs located in different angular positions around node 1. The position of the kth UE is defined by a pair of angles $\{\phi_k, \theta_k\}$ ($k \in \Omega_{UEs}$ with $\Omega_{UEs} = \{UE0, UE1, UE2\}$), where ϕ_k and θ_k represent the elevation and azimuth angles of the kth UE. The distance d_{UEk} between each UE and node 1 is also considered. Adjacent nodes are

TABLE 1. Simulation parameters in MATLAB for UEs UL scenario.

Symbol	Quantity	Value
K_1	Number of UEs around node 1	3
$M_{\mathrm{R_x}}^{(1)}$	Number of R_x antennas at node 1	32
$M_{\mathrm{R_x,BH}}^{(1)}$	Number of R_x antennas at node 1 for BH signal	8
$M_{\mathrm{R_x,UE_k}}^{(1)}$	Number of R_x antennas at node 1 for the kth UE ($k \in \{0,1,2\}$)	8
$M_{\mathrm{T_x}}^{(1)}$	Number of T_x antennas at node 1	32
$M_{\mathrm{T_x,BH}}^{(1)}$	Number of T_x antennas at node 1 for BH signal	8
$M_{\mathrm{T_x,BH}}^{(0)}$	Number of T_x antennas at node 0 for BH signal	8
$M_{\mathrm{R_x,BH}}^{(2)}$	Number of R_x antennas at node 2 for BH signal	8
B	Bandwidth	400MHz
f	Central frequency	28GHz
$h_{\mathrm{node_1}}$	Height of node 1	35m
$d_{n \leftrightarrow n+1}$	Distance between the adjacent nodes ($n \in \{0,1\}$)	100m
$D^{(1)}$	Distance between the center of T_x and R_x array at node 1	1m
d_{UE0}	Distance between node 1 and UE0	20m
d_{UE1}	Distance between node 1 and UE1	10m
d_{UE2}	Distance between node 1 and UE2	40m
ϕ_{tilt}	Angle of rotation between T_x and R_x array at node 1	10°
$\{\phi_{\mathrm{BH}}^{(0)}, \theta_{\mathrm{BH}}^{(0)}\}$	Elevation and azimuth angle of BH antennas of node 0	$\{0°, 10°\}$
$\{\phi_{\mathrm{BH}}^{(1)}, \theta_{\mathrm{BH}}^{(1)}\}$	Elevation and azimuth angle of BH antennas of node 2	$\{10°, -45°\}$
$\{\phi_{\mathrm{UE0}}, \theta_{\mathrm{UE0}}\}$	Elevation and azimuth angle of UE0	$\{-30°, -60°\}$
$\{\phi_{\mathrm{UE1}}, \theta_{\mathrm{UE1}}\}$	Elevation and azimuth angle of UE1	$\{-30°, 0°\}$
$\{\phi_{\mathrm{UE2}}, \theta_{\mathrm{UE2}}\}$	Elevation and azimuth angle of UE2	$\{-30°, 60°\}$
P_{BH}	Transmitted power for BH signal	50W
P_{UE}	Transmitted power for UE signals	1W

separated by a distance of 100m, and node 1 in particular has a height of 35m. Moreover, we assume that each node has 2 UPAs, with 32 elementary antennas on both T_x and R_x. A separation of 1m between the center of the R_x UPA and the T_x UPA at node 1 is considered. To accurately model the SI channel between the T_x and R_x of node 1, a tilt angle of 10° is applied between the two arrays so that the R_x of node 1 is in the propagation view of T_x of node 1. The R_x of node 1 employs for each transmitter (UEs and node 0) 8 elementary antennas to receive the SOI. Similarly, the T_x of node 0 employs 8 antennas to transmit the BH signal to node 1, as the T_x of node 1 and R_x of node 2 employs 8 antennas to transmit the BH signal to node 2 and receive the BH signal from node 1, respectively. Furthermore, the elementary antennas dedicated to receiving UEs' UL signals are positioned below those for BH signal reception,

with the order from top to bottom as follows: UE0 signal reception, UE1 signal reception, and UE2 signal reception. Finally, the BH signals are transmitted with a power of 50W, while signals from UEs are sent with a power of 1W. Our simulation adhere to typical 5G mmWave conditions, with a central frequency of 28GHz and a bandwidth of 400MHz.

The primary metric used to evaluate the effectiveness of our method is the SE for receiving both the BH signal and UL signals from UEs at node 1. The SE for the reception of the signal k ($\forall k \in \{\mathrm{BH0} \to 1\} \cup \Omega_{\mathrm{UEs}}$) at node 1, denoted as $\mathrm{SE}_k^{(1)}$, is computed using the following expression:

$$\mathrm{SE}_k^{(1)} = \log_2 \left(1 + \frac{P_{\mathrm{SOI},k}^{(1)}}{P_{\mathrm{noise},k}^{(1)} + P_{\mathrm{SI},k}^{(1)} + P_{\mathrm{int},k'}^{(1)}} \right), \qquad (39)$$

with $P_{\mathrm{SOI},k}^{(1)}$ representing the power of the received SOI k at node 1. Additionally, $P_{\mathrm{noise},k}^{(1)}$ accounts for the received noise power during the reception of SOI k at node 1. Furthermore, $P_{\mathrm{SI},k}^{(1)}$ denotes the power of the received SI signal associated with the reception of SOI k at node 1. Lastly, $P_{\mathrm{int},k'}^{(1)}$ represents the power of the sum of the received interference signal, where k' varies and excludes k ($\forall k' \in \{\mathrm{BH0} \to 1\} \cup \Omega_{\mathrm{UEs}} \backslash k$).

B. SIMULATION RESULTS
Firstly, in Fig. 6, we compare the SE performance versus SNR (defined as the ratio between P_{SOI} and P_{noise}) to evaluate the reception of the BH link from node 0 at the R_x of node 1. The comparison includes three proposed beamforming schemes: the modified ZF beamforming defined by (21), the modified MMSE beamforming scheme defined by (25), and the C-MMSE beamforming scheme defined by (37). In Fig. 6-(a), the SNR range is limited from -5dB to 40dB, and in Fig. 6-(b), we explore a higher SNR range (from 55dB to 85dB) to analyze the asymptotic behavior of the proposed beamforming methods. Across both figures, it is obvious that all three proposed beamforming schemes effectively perform SIC. More precisely, the C-MMSE outperforms the modified ZF scheme, showing the best behavior in terms of BH signal reception. The difference between C-MMSE and the modified ZF scheme is consistently notable, with a constant difference of 1.6 bps/Hz observed in the SNR range between 10 and 30 dB. Additionally, the performance difference between the C-MMSE and the modified MMSE varies. For low SNR values (up to 12 dB), the modified MMSE scheme exhibits the worst behavior in terms of SE. However, at higher SNR values, the modified MMSE scheme surpasses the modified ZF scheme, asymptotically approaching the performance of the C-MMSE scheme. It is essential to note that the modified MMSE combiner converges with the modified ZF combiner as the noise power σ^2 tends to almost null. In the high SNR region (Fig. 6-(b)), the modified MMSE scheme effectively converges to the modified ZF scheme. However, the C-MMSE scheme demonstrates a higher asymptotic value than the other two methods (a slight
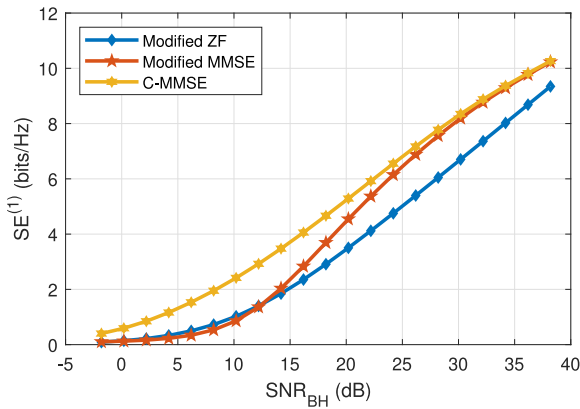
(a) Comparison of the 3 proposed beamforming methods for the reception of BH signal in nominal SNR region.
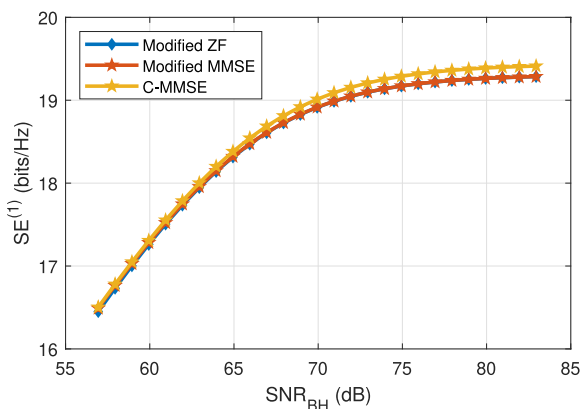
(b) Comparison of the 3 proposed beamforming methods for the reception of the BH signal in asymptotic SNR region.

FIGURE 6. Comparison of SE vs SNR_{BH} of the reception of the BH link at node 1 between the proposed modified ZF beamforming, the proposed modified MMSE beamforming and the proposed C-MMSE beamforming in the UEs UL scenario.

difference of 0.13bps/Hz can be observed at SNR=83dB), indicating superior SI cancellation ability. In conclusion, all three proposed combining schemes effectively cancel the SI, ensuring good reception of the BH signal in FD operation. However, the C-MMSE combiner outperforms the others in terms of SIC.

After evaluating the performance of the different combiners for the reception of the BH signal, we turn our attention to Fig. 7, where we analyze the sum rate performance of the UEs' UL signal versus the parameter $\frac{1}{\sigma^2}$. It is important to note that due to the distinct definition of SNR for each received signal in the R_x array, we opt to use $\frac{1}{\sigma^2}$ on the x-axis instead of SNR for better illustration of the reality. The sum rate, denoted as $\Sigma^{(1)}$, is defined as follows:

$$\Sigma^{(1)} = \sum_{k \in \Omega_{UEs}} SE_k^{(1)}. \tag{40}$$

As we can observe in Fig. 7, the modified ZF combiner outperforms both MMSE-based combiners for values of $\frac{1}{\sigma^2}$ below -6.5×10^{-3}dBm. In the entire considered $\frac{1}{\sigma^2}$ range,
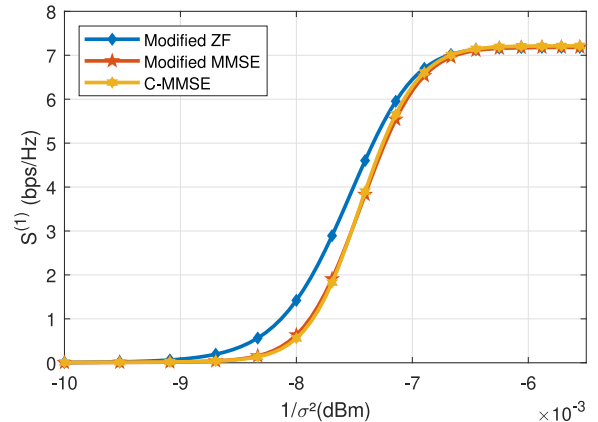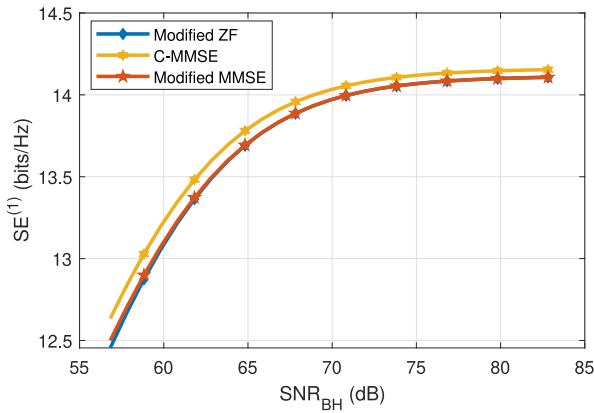

FIGURE 7. Comparison of the 3 proposed beamforming methods for the UEs UL signal sum rate.

the modified MMSE and C-MMSE exhibits similar behavior. This observation can be explained by the fact that the modified ZF combiner effectively cancels both the SI power $P_{SI,k}^{(1)}$ and interference power $P_{int,k'}^{(1)}$, resulting in higher SE as the noise power decreases. On the other hand, for the modified MMSE and C-MMSE combiners, only the SI power $P_{SI,k}^{(1)}$ is canceled, and the interference power becomes the major source of degradation in the final SE. Besides, for values of $\frac{1}{\sigma^2}$ above -6.5×10^{-3}dBm, a pattern similar to the previous analysis emerges: the ZF combiner approaches the same asymptotic value as the modified MMSE combiner. In conclusion, all three proposed combiners effectively perform SIC, while the modified ZF combiner leads in terms sum rate for the reception of the UEs' UL signal.

Next in Fig. 8, we further evaluate the SIC capability of our proposed combiners by significantly increasing the power of the BH link transmission at node 1 (from 50W to 500W). This power increase precisely represents the source of SI. Similar to Fig. 6, we analyze the behavior of the three combiners' in terms of SE versus SNR in a nominal (Fig. 8-(a)) and high SNR region (8-(b)). In both Fig. 8-(a) and Fig. 8-(b), due to the higher amount of transmit SI power, the overall performance is degraded, resulting in a lower achievable SE compared to Fig. 6-(a) and Fig. 6-(b). In Fig. 8-(a), the global behavior of the three combiners aligns with Fig. 6-(a): the proposed C-MMSE combiner consistently outperforms the modified MMSE and modified ZF combiner throughout the nominal SNR range (a difference of 1bps/Hz can be observed between the SE of the C-MMSE combiner and the modified ZF and modified MMSE). Notably, when the transmit SI power is increased, the modified ZF combiner achieves a higher SE than the modified MMSE combiner accross the entire nominal SNR range. This highlights the limitation of the modified MMSE combiner: without explicit SIC constraints during its design, it struggles to perform SIC effectively in the considered nominal SNR range when SI is substantial. In contrast, the C-MMSE excels in SIC and simultaneously reduces additive
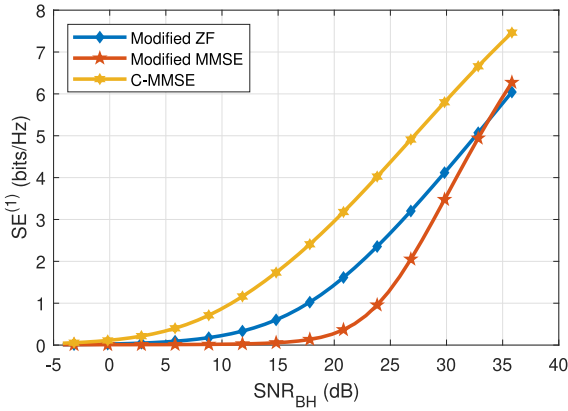
(a) Comparison of the 3 proposed beamforming methods for the reception of BH signal in nominal SNR region. ($P_{SI} = 500W$)
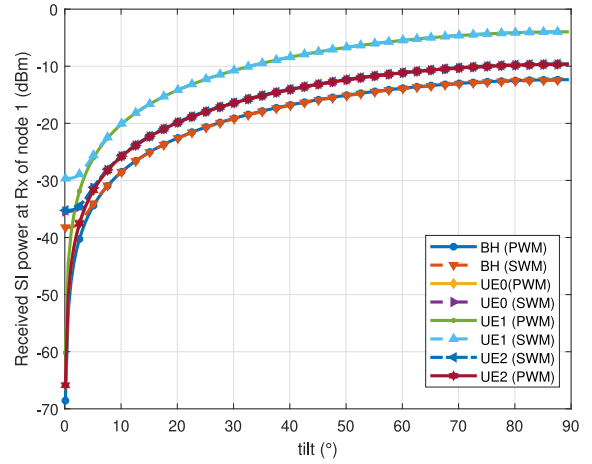

(b) Comparison of the 3 proposed beamforming methods for the reception of the BH signal in asymptotic SNR region. ($P_{SI} = 500W$)
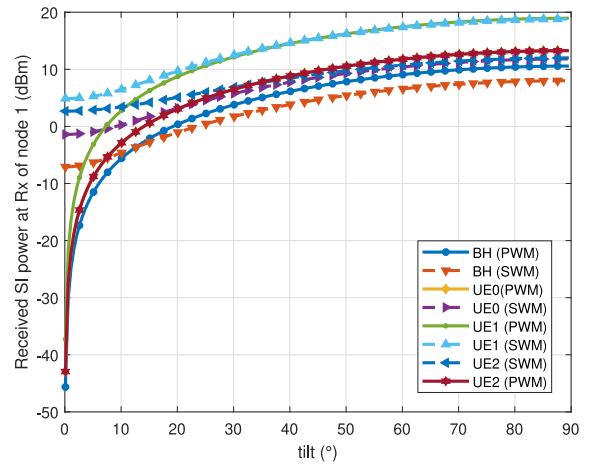
FIGURE 8. Comparison of SE vs SNR_{BH} of the reception of the BH link at node 1 between the proposed modified ZF beamforming, the proposed modified MMSE beamforming and the proposed C-MMSE beamforming in the UEs UL scenario.

(a) Comparison of the received SI power with PWM and SWM for the different elementary antennas with only analog beamforming at R_x of node 1 at 28GHz
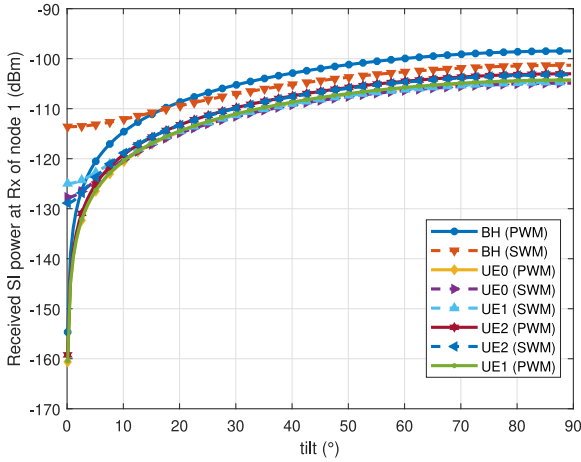

(b) Comparison of the received SI power with PWM and SWM for the different elementary antennas with only analog beamforming at R_x of node 1 at 2GHz
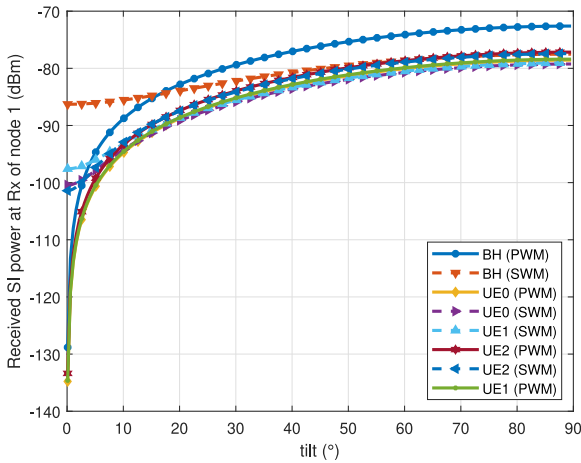
FIGURE 9. Comparison of the received SI power with PWM and SWM for the different elementary antennas with only analog beamforming at R_x of node 1 at different carrier frequency.

noise distortion. Moving to Fig. 8-(b), we focus on analyzing the asymptotic behavior of the three combiners. Similar to Fig. 6-(b), the C-MMSE combiner exhibits a higher asymptotic value than the modified ZF and modified MMSE combiner, while the latter two have the same asymptotic value. Beyond the previously drawn conclusions, we observe that when faced with a high amount of SI power, even though the three considered combiners can perform SIC, the C-MMSE combiner proves to be more robust than the modified ZF and modified MMSE combiners.

Finally, we evaluate the relevance of using SWM to model the SI channel in comparison to the commonly used PWM. In Fig. 9, we examine the received SI power at different elementary antennas of the R_x at node 1 with only analog beamforming at 28GHz and 2GHz. In Fig. 9-(a), at 28GHz, both PWM and SWM exhibits very similar behavior. However, for tilt angles less than 5°, we observe that the received SI power with PWM rapidly diminishes for a tilt angle close to 0°. In contrast, with SWM, the received SI power remains non-null for small tilt angles. This observation highlights the accuracy of the SWM compared to the PWM. The behavior of the PWM, where the received SI power is almost null without any tilt, is inconsistent with practical scenarios. Additionally, we observe that the antennas dedicated to receiving the UL signal from UE1 receive the most SI, while those dedicated to the BH signal reception from node 0 receive the least. This discrepancy can be explained by the fact that the antennas for UE1 signal reception, with a direction of 0° for the azimuth angle, are directly exposed to the radiation of the T_x array when it rotates. On the other hand, antennas receiving the BH signal are placed on top of the R_x array, above the T_x array (as illustrated in Fig. 1), resulting in the furthest distance from the source of SI and thus, the minimum amount of SI received. Moving to Fig. 9-(b), the difference between both

(a) Comparison of the received SI power with PWM and SWM for the different elementary antennas with hybrid beamforming at R_x of node 1 at 28GHz (C-MMSE hybrid beamforming)

(b) Comparison of the received SI power with PWM and SWM for the different elementary antennas with hybrid beamforming at R_x of node 1 at 2GHz (C-MMSE hybrid beamforming)

FIGURE 10. Comparison of the received SI power with PWM and SWM for the different elementary antennas with hybrid beamforming at R_x of node 1 at different carrier frequency.

SWM and PWM becomes more pronounced, but the overall behavior of both models remains similar to 9-(a).

In this final evaluation, we examine the received SI power at the R_x of node 1, including this time a BB combiner. The selected combiner is the C-MMSE, as its SIC performance has been proven to be the highest among all the proposed digital combiners. Similar to Fig. 9, we compare the situations with the carrier frequency set at 28GHz and 2GHz. In Fig. 10, we observe the effects of the C-MMSE combiner in both 10-(a) and Fig. 10-(b). Compared to the situation with only analog beamforming in Fig. 9, we notice significantly lower received SI power due to the additional constraints imposed to cancel the SI. More precisely, in both Fig. 10-(a) and Fig. 10-(b), at 28GHz and 2GHz, the

proposed C-MMSE combiner is capable of canceling an average of 90dB of SI power. This result proves once again the robustness of the proposed C-MMSE combiner in terms of SIC across different frequency bands. Furthermore, we observe the same behavior between SWM and PWM as in Fig. 9. The PWM exhibits fading behavior for tilt angles close to 0°, while the SWM shows smoother variations that align closer to reality. This observation holds true regardless of the chosen frequency, advocating for the use of the SWM for accurate performance evaluation.

VI. CONCLUSION

In this paper, we have introduced a spatial domain-based SIC method called C-MMSE, designed to cancel SI in a MIMO FD system in a UL scenario for UEs. We adapted traditional combining schemes, such as ZF combining and MMSE combining to our specific system and showed that our proposed C-MMSE combiner outperforms the modified ZF and the modified MMSE in terms of SIC. Our theoretical analysis, complemented by simulations, revealed that the SIC capability of the modified MMSE combiner is inferior to that of C-MMSE, which achieves perfect SIC. Moreover, despite the high performance of the modified ZF combiner regarding the UE sum rate, the C-MMSE combiner is able to reach higher asymptotic SE values than the latter. In addition to the new combiner design and related results, the relevance of the SWM compared to the PWM for the SI channel model has also been highlighted through simulations. Accurate SI channel models becomes crucial, especially as our proposed C-MMSE strategy effectively reduces the power of SI signal. In future work, we plan to extend our investigation to a comprehensive scenario involving both UL and DL traffic for UEs. We aim to propose a joint design for both the T_x and R_x parts. More complex designs, such as fully-connected RF chains for analog precoder/combiner, consideration of hardware impairments in the system model, and consideration of channel errors for the precoder/combiner, are also in the scope of our ongoing research.

APPENDIX
PROOF OF (38)

Proof: We evaluate the first column of the resulting matrix $W_{BB,C-MMSE}^H H_{eq}$ to show the effect of the proposed C-MMSE combiner. To provide a more detailed expression of (36), we introduce the following quantity:

$$\gamma = H_{eq}^H \left(H_{eq} H_{eq}^H + \sigma^2 I \right)^{-1} H_{eq} c_0, \tag{41}$$

with γ a $(K_1 + 2) \times 1$ vector. The expression of (36) can then be expressed as:

$$\forall k \in \{0, \dots, K_1 + 1\}: \mu_k = \frac{\alpha_k}{\Gamma} = \frac{j_k^T A_{ZF} \gamma}{c_0^T \gamma}. \tag{42}$$

Due to the construction of j_k and A_{ZF}, the following expression can be deduced:

$$\forall k \in \{0, \dots, K_1 + 1\}: j_k^T A_{ZF} = c_{k+1}^T, \tag{43}$$

thus, (36) can be written only with the rows of $\boldsymbol{\gamma}$:

$$\forall k \in \{0, \ldots, K_1 + 1\} : \mu_k = \frac{\boldsymbol{\gamma}_{k+1}}{\boldsymbol{\gamma}_0}, \qquad (44)$$

with $\boldsymbol{\gamma}_{k+1}$ the $(k+2)$th row of $\boldsymbol{\gamma}$ and $\boldsymbol{\gamma}_0$ the first row of $\boldsymbol{\gamma}$.

We now examine the first column of the resulting matrix $\boldsymbol{W}_{\mathrm{BB,C-MMSE}}^H \boldsymbol{H}_{\mathrm{eq}}$ with the newly defined μ_k to evaluate the effect of SIC. To isolate the first column of $\boldsymbol{W}_{\mathrm{BB,C-MMSE}}^H \boldsymbol{H}_{\mathrm{eq}}$, we calculate $\boldsymbol{W}_{\mathrm{BB,C-MMSE}}^H \boldsymbol{H}_{\mathrm{eq}} \boldsymbol{c}_0$, resulting in:

$$\boldsymbol{W}_{\mathrm{BB,C-MMSE}}^H \boldsymbol{H}_{\mathrm{eq}} \boldsymbol{c}_0 = \left(\boldsymbol{A}_{\mathrm{ZF}} \boldsymbol{H}_{\mathrm{eq}}^H - \sum_{k=0}^{K_1} \frac{\boldsymbol{\gamma}_{k+1}}{\boldsymbol{\gamma}_0} \boldsymbol{j}_k \boldsymbol{c}_0^T \boldsymbol{H}_{\mathrm{eq}} \right)$$
$$\left(\boldsymbol{H}_{\mathrm{eq}} \boldsymbol{H}_{\mathrm{eq}}^H + \sigma^2 \boldsymbol{I} \right)^{-1} \boldsymbol{H}_{\mathrm{eq}} \boldsymbol{c}_0$$
$$= \boldsymbol{A}_{\mathrm{ZF}} \boldsymbol{\gamma} - \sum_{k=0}^{K_1} \boldsymbol{\gamma}_{k+1} \boldsymbol{j}_k$$
$$= \boldsymbol{0}. \qquad (45)$$

An interesting observation arises here. Equation (45) is a difference between two terms: the first term, $\boldsymbol{A}_{\mathrm{ZF}} \boldsymbol{\gamma}$, corresponds to the effect of the modified MMSE combiner calculated in (25), while the second term, $\sum_{k=0}^{K_1} \boldsymbol{\gamma}_{k+1} \boldsymbol{j}_k$, accounts for the impact of the $K_1 + 1$ constraints we introduced. Mathematically, we observe that the modified MMSE combiner in (25) is unable to cancel the SI signal, as the term $\boldsymbol{A}_{\mathrm{ZF}} \boldsymbol{\gamma} = (\gamma_1, \ldots, \gamma_{K_1+1})^T$ is different from the null vector. However, with the additional constraints expressed by the second term in (45), the SI contribution at the RF chains of $\mathrm{R_x}$ of node 1 is systematically eliminated one by one due to the sum operator. ∎

REFERENCES

[1] H. Alves, T. Riihonen, and H. A. Suraweera, *Full-Duplex Communications for Future Wireless Networks*. Singapore: Springer, 2020.

[2] A. Sabharwal, P. Schniter, D. Guo, D. W. Bliss, S. Rangarajan, and R. Wichman, "In-band full-duplex wireless: Challenges and opportunities," *IEEE J. Sel. Areas Commun.*, vol. 32, no. 9, pp. 1637–1652, Sep. 2014.

[3] N. Mahmood, M. Gatnau Sarret, G. Berardinelli, and P. Mogensen, "Full duplex communications in 5G small cells," in *Proc. IWCMC*, Jun. 2017, pp. 1665–1670.

[4] T. Dinc and H. Krishnaswamy, "Millimeter-wave full-duplex wireless: Applications, antenna interfaces and systems," in *Proc. IEEE Custom Integr. Circuits Conf. (CICC)*, 2017, pp. 1–8.

[5] G. Liu, F. R. Yu, H. Ji, V. C. M. Leung, and X. Li, "In-band full-duplex relaying: A survey, research issues and challenges," *IEEE Commun. Surveys Tuts.*, vol. 17, no. 2, pp. 500–524, 2nd Quart., 2015.

[6] D. Bharadia, E. McMilin, and S. Katti, "Full duplex radios," *SIGCOMM Comput. Commun. Rev.*, vol. 43, no. 4, pp. 375–386, Aug. 2013. [Online]. Available: https://doi.org/10.1145/2534169.2486033

[7] T. Riihonen, S. Werner, and R. Wichman, "Spatial loop interference suppression in full-duplex MIMO relays," in *Proc. Rec. 43rd Asilomar Conf. Signals, Syst. Comput.*, 2009, pp. 1508–1512.

[8] J.-H. Lee and O.-S. Shin, "Full-duplex relay based on block diagonalisation in multiple-input multiple-output relay systems," *IET Commun.*, vol. 4, pp. 1817–1826, Nov. 2010.

[9] Y. Sung, J. Ahn, B. V. Nguyen, and K. Kim, "Loop-interference suppression strategies using antenna selection in full-duplex MIMO relays," in *Proc. Int. Symp. Intell. Signal Process. Commun. Syst. (ISPACS)*, 2011, pp. 1–4.

[10] A. Bishnu, M. Holm, and T. Ratnarajah, "Performance evaluation of full-duplex IAB multi-cell and multi-user network for FR2 band," *IEEE Access*, vol. 9, pp. 72269–72283, 2021.

[11] J. Zhang, N. Garg, and T. Ratnarajah, "In-band-full-duplex integrated sensing and communications for IAB networks," *IEEE Trans. Veh. Technol.*, vol. 71, no. 12, pp. 12782–12796, Dec. 2022.

[12] X. Han et al., "Interference mitigation for non-overlapping sub-band full duplex for 5G-advanced wireless networks," *IEEE Access*, vol. 10, pp. 134512–134524, 2022.

[13] M. Chafii, L. Bariah, S. Muhaidat, and M. Debbah, "Twelve scientific challenges for 6G: Rethinking the foundations of communications theory," *IEEE Commun. Surveys Tuts.*, vol. 25, no. 2, pp. 868–904, 2nd Quart., 2023.

[14] C. D. Nwankwo, L. Zhang, A. Quddus, M. A. Imran, and R. Tafazolli, "A survey of self-interference management techniques for single frequency full duplex systems," *IEEE Access*, vol. 6, pp. 30242–30268, 2018.

[15] D. Kim, H. Lee, and D. Hong, "A survey of in-band full-duplex transmission: From the perspective of PHY and MAC layers," *IEEE Commun. Surveys Tuts.*, vol. 17, no. 4, pp. 2017–2046, 4th Quart., 2015.

[16] C. R. Anderson et al., "Antenna isolation, wideband multipath propagation measurements, and interference mitigation for on-frequency repeaters," in *Proc. IEEE SoutheastCon*, 2004, pp. 110–114.

[17] M. Duarte and A. Sabharwal, "Full-duplex wireless communications using off-the-shelf radios: Feasibility and first results," in *Proc. Conf. Rec. 44th Asilomar Conf. Signals, Syst. Comput.*, 2010, pp. 1558–1562.

[18] J. I. Choi, M. Jain, K. Srinivasan, P. Levis, and S. Katti, "Achieving single channel, full duplex wireless communication," in *Proc. 16th Annu. Int. Conf. Mobile Comput. Netw.*, 2010, pp. 1–12. [Online]. Available: https://doi.org/10.1145/1859995.1859997

[19] M. Duarte, C. Dick, and A. Sabharwal, "Experiment-driven characterization of full-duplex wireless systems," *IEEE Trans. Wireless Commun.*, vol. 11, no. 12, pp. 4296–4307, Dec. 2012.

[20] B. Radunovic et al., "Rethinking indoor wireless mesh design: Low power, low frequency, full-duplex," in *Proc. 5th IEEE Workshop Wireless Mesh Netw.*, 2010, pp. 1–6.

[21] M. Jain et al., "Practical, real-time, full duplex wireless," in *Proc. MobiCom*, Sep. 2011, pp. 301–312.

[22] A. Sahai, G. Patel, and A. Sabharwal, "Pushing the limits of full-duplex: Design and real-time implementation," Jul. 2011, *arXiv:1107.0607*.

[23] R. Lopez-Valcarce, E. Antonio-Rodriguez, C. Mosquera, and F. Perez-Gonzalez, "An adaptive feedback canceller for full-duplex relays based on spectrum shaping," *IEEE J. Sel. Areas Commun.*, vol. 30, no. 8, pp. 1566–1577, Sep. 2012.

[24] S. Li and R. D. Murch, "An investigation into baseband techniques for single-channel full-duplex wireless communication systems," *IEEE Trans. Wireless Commun.*, vol. 13, no. 9, pp. 4794–4806, Sep. 2014.

[25] D. Bharadia, E. McMilin, and S. Katti, "Full duplex radios," in *Proc. ACM SIGCOMM Conf. SIGCOMM*, 2013, pp. 375–386. [Online]. Available: https://doi.org/10.1145/2486001.2486033

[26] B. Chun, E.-R. Jeong, J. Joung, Y. Oh, and Y.-H. Lee, "Pre-Nulling for self-interference suppression in full-duplex relays," in *Proc. APSIPA Annu. Summit Conf.*, 2009, pp. 91–97.

[27] T. Riihonen, S. Werner, and R. Wichman, "Mitigation of loopback self-interference in full-duplex MIMO relays," *IEEE Trans. Signal Process.*, vol. 59, no. 12, pp. 5983–5993, Dec. 2011.

[28] C. K. Sheemar and D. Slock, "Massive MIMO mmWave full duplex relay for IAB with limited dynamic range," in *Proc. 11th IFIP Int. Conf. New Technol., Mobility Security (NTMS)*, 2021, pp. 1–5.

[29] T. Riihonen, A. Balakrishnan, K. Haneda, S. Wyne, S. Werner, and R. Wichman, "Optimal eigenbeamforming for suppressing self-interference in full-duplex MIMO relays," in *Proc. 45th Annu. Conf. Inf. Sci. Syst.*, 2011, pp. 1–6.

[30] K. Satyanarayana, M. El-Hajjar, P.-H. Kuo, A. Mourad, and L. Hanzo, "Hybrid beamforming design for full-duplex Millimeter wave communication," *IEEE Trans. Veh. Technol.*, vol. 68, no. 2, pp. 1394–1404, Feb. 2019.

[31] J.-S. Jiang and M. A. Weitnauer, "Spherical-wave model for short-range MIMO," *IEEE Trans. Commun.*, vol. 53, pp. 1534–1541, Sep. 2005.

[32] X. Chen, V. Savaux, M. Crussieres, P. Savelli, and K.-C. Yao, "Influence of the self-interference channel model on the performance of a full-duplex MIMO system," in *Proc. IEEE Global Commun. Conf.*, Kuala Lumpur, Malaysia, Dec. 2023, pp. 1–7.

[33] S. Gadhai and R. Budhiraja. "Evolution of network nodes: From IAB to IRS." 2023. [Online]. Available: https://www.3gpp.org/news-events/partner-news/iab-irs

[34] Y. Zhou, "On the performance of spatial modulation and full duplex radio architectures," M.S. thesis, Électronique, Électrotechnique, Automatique, Université de Lyon, Lyon, France, Dec. 2021. [Online]. Available: https://tel.archives-ouvertes.fr/tel-03506890

[35] A. L. Calvez, L. L. Magoarou, and S. Paquelet, "Massive MIMO channel estimation taking into account spherical waves," 2018, *arXiv:1811.05669*.

[36] A. Roze, M. Crussière, M. Helard, and C. Langlais, "Comparison between a hybrid digital and analog beamforming system and a fully digital massive MIMO system with adaptive beamsteering receivers in millimeter-wave transmissions," in *Proc. Int. Symp. Wireless Commun. Syst. (ISWCS)*, Sep. 2016, pp. 86–91.

[37] G. Y. Suk, S.-M. Kim, J. Kwak, S. Hur, E. Kim, and C.-B. Chae, "Full duplex integrated access and backhaul for 5G NR: Analyses and prototype measurements," *IEEE Wireless Commun.*, vol. 29, no. 4, pp. 40–46, Aug. 2022.

[38] K. B. Petersen and M. S. Pedersen, "The matrix cookbook, version 20121115." Nov. 2012. [Online]. Available: http://www2.compute.dtu.dk/pubdb/pubs/3274-full.html

[39] A. Hjorungnes and D. Gesbert, "Complex-valued matrix differentiation: Techniques and key results," *IEEE Trans. Signal Process.*, vol. 55, no. 6, pp. 2740–2746, Jun. 2007.